Inorganic Chemistry

Article

pubs.acs.org/IC

Large Oxygen Nonstoichiometry in $La_{0.77}Sr_{3.23}Co_{2.75}C_{0.25}O_{8.40+\delta}$ Oxide (δ = 0, 1.3) Related to n = 3 RP Series

A. Demont,[†] S. Hébert,[†] J. Höwing,[‡] Y. Bréard,[†] and D. Pelloquin*,[†]

[†]Laboratoire CRISMAT, UMR CNRS-ENSI Caen 6508, 6 bd Maréchal Juin, 14050 CAEN Cedex, France

[‡]Institute for Energy Technology, P.O. Box 40, Kjeller NO-2027, Norway

Supporting Information

ABSTRACT: An original Ruddlesden–Popper phase, $La_{0.77}Sr_{3.23}Co_{2.75}C_{0.25}O_{8.40+\delta}$, was isolated and studied by electron, X-ray, and neutron diffraction. This structure has complex crystal chemistry resulting from a high degree of flexibility in the structure, comprising the disordered introduction of carbonates into a cobalt layer and an important oxygen deficiency with a preferential repartition of vacancies along the layers stacking sequence. The former is necessary for the stabilization of the system, while the latter can be tuned by postsynthetic treatment, yielding in a large variety of cobalt species formal oxidation states ranging from Co^{2+}/Co^{3+} in the as-made phase to Co^{3+}/Co^{4+} when annealed under oxygen pressure. The potential richness deriving from this flexibility is illustrated in terms of the magnetotransport properties and includes a resistivity that varies within a range of 5 orders of magnitude after modulation of the oxygen content with the appearance of negative magnetoresistance and ferromagnetic interactions due to Co^{3+}/Co^{4+} mixed-valence state.

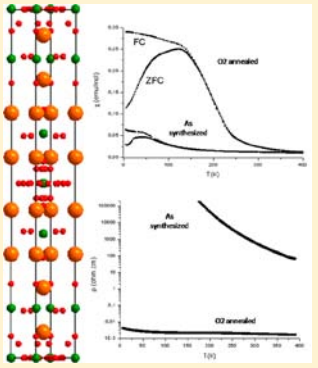

INTRODUCTION

Transition metal oxides are a preponderant class of functional materials, being competitive or dominant in a wide array of application fields.[1−4] Among them, cobalt oxides display a richness of behaviors that has attracted considerable attention,[5] from fundamental[6,7] to applicative research.[8−10] Indeed, the flexibility of the perovskite structure and variety of cobalt oxidation states deliver great potential for tuning both crystal chemistry and physical properties. However, one should note an oddity in the emergence of studies concerning cobalt perovskites when compared with the historical emergence of copper and manganese perovskites, studied for their high T_c superconductivity[11] and colossal magnetoresistance.[12,13] For instance, the search for high-T_c superconductors was accompanied with a large quantity of studies on structure types with a layered character, derived from the perovskite. Hence, these parent materials had a major role in the discovery of new high-performing materials,[14−16] and to date, the compound with the highest superconducting T_c is in fact not a perovskite but one of its derivates, $HgBa_2Ca_2Cu_3O_{8+\delta}$.[17] Layered compounds were then regarded as being highly attractive as well, offering a comparable degree of flexibility toward phenomena such as chemical substitutions or oxygen nonstoichiometry, which are of predominant importance for control of physical properties. It is therefore surprising that perovskite derivates such as Ruddlesden–Popper (RP) phases $A_{n+1}B_nO_{3n+1}$[18] have so far attracted marginal attention in the case of cobalt oxides, while cobalt-containing perovskites are considered as predominant materials in emerging technologies.[5,19]

Moreover, existing studies have already demonstrated the flexibility of RP2 cobalt frameworks from a structural point of view[20−24] with incorporation of large amounts of oxygen vacancies while cobalt is retained in a mixed-valent state. In addition to the display of interesting magnetotransport properties, such compounds could be promising for generation of gas-separating membranes where mixed ionic–electronic conductivity is required. However the title RP2 system, $Sr_3Co_2O_{7-\delta}$, has also been shown to form hydrated oxihydroxydes,[25] which makes it unstable after extended time under air exposure. The cobalt RP family was also extended with a RP3 that has been reported in the form of $Ln_4Co_3O_{10}$ (Ln = La^{3+}, Nd^{3+}).[26,27] Nevertheless, this compound displays less opportunity to tune the oxygen content and cobalt oxidation state than formerly observed in the Sr-rich RP2 frameworks. To date, no alkaline-earth-rich cobalt RP3 has been reported, most probably due to competition with phases such as the RP2 or hexagonal perovskite derivates.[28] This difficulty to obtain such compound is probably best exemplified by $Sr_4Co_3O_9$,[29,30] which has the ideal stoichiometry to form an oxygen-deficient RP3 $Sr_4Co_3O_{10-\delta}$ but crystallizes in a hexagonal perovskite-derived stacking. More recently, the report of an oxygen-deficient $Sr_4Co_2(CO_3)O_{6-\delta}$ phase[31] opened a door toward stabilization of new cobalt-rich compounds related to the framework of a RP3 phase. Formation of this oxycarbonate rather than the aforementioned competing phases in the Sr–Co–O system suggests that carbonates introduction plays a major role in the stabilization of high-n RP members.

Further work in order to utilize the carbonates role in formation of RP3-related frameworks is reported here. The

Received: August 12, 2012
Published: January 14, 2013

   dx.doi.org/10.1021/ic3017694 | Inorg. Chem. 2013, 52, 1265−1274

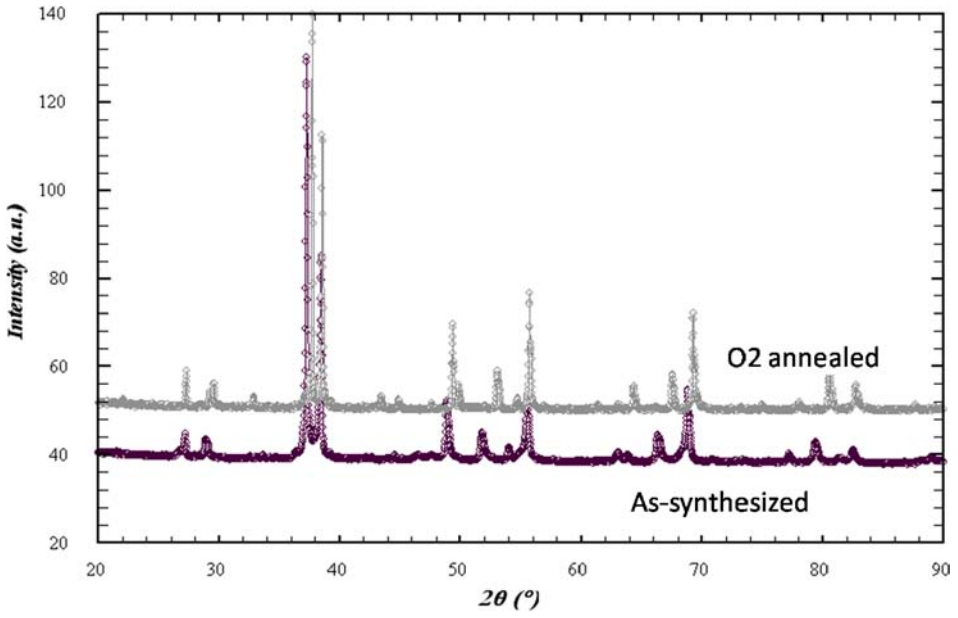

Figure 1. Evolution of powder X-ray diffraction pattern after oxidizing annealing under P_{O_2} = 10 MPa.

complex interplay between allovalent A-site substitution (La^{3+} for Sr^{2+}), carbonate content, cobalt formal oxidation state, and oxygen nonstoichiometry indeed allowed isolating new Co-rich layered phases. This article is therefore devoted to the study of a new n = 3 member of the RP series, namely, $Sr_{3.23}La_{0.77}Co_{2.75}C_{0.25}O_{8.40+\delta}$. A wide range of oxygen nonstoichiometry (δ) is demonstrated from oxidizing annealing, and its impact is studied on both the structural and the physical properties, showing dramatic variations in the compound behavior.

EXPERIMENTAL SECTION

1. As-Synthesized Material. Polycrystalline sample was obtained from solid state reactions of SrO, $SrCO_3$, La_2O_3, and Co_3O_4 in respective stoichiometric proportions of 3.05, 0.25, 0.35, and 11/12, giving the nominal composition $Sr_{3.3}La_{0.7}Co_{2.75}(CO_3)_{0.25}O_{7.77}$. SrO and La_2O_3 were stored, respectively, at 1200 and 900 °C in order to avoid formation of strontium carbonate for the former and lanthanum hydroxide for the latter and introduced while still incandescent in a nitrogen-filled glovebox where they were intimately mixed with other powders before being pressed in the form of bars, later introduced in point bottom alumina crucibles with circular section, and sealed in silica tubes previously pumped under primary vacuum. The reaction was then performed at 1150 °C for 24 h followed by quenching to room temperature.

2. Oxidized Material. Black ceramic bars of the as-synthesized material were annealed at 400 °C for 24 h under O_2 with a pressure of 10 MPa. Cooling to room temperature was performed in 6 h.

For both the as-synthesized and the oxidized materials these synthetic treatments allowed reproducible single-phase samples (controlled by powder X-ray diffraction) on a scale of 0.8 g. These samples were used for all characterizations except the neutron diffraction experiments. A scaling up to 5 g for the neutron diffraction experiment resulted in observation of 3% of (La,Sr)CoO_3 and 2% of (La,Sr)CoO_4 as impurity phases (in weight) for the as-synthesized and oxidized samples, respectively.

Preliminary structural characterizations were carried out by powder X-ray diffraction on a Panalytical X'Pert Pro diffractometer working with Co Kα radiation. Electron diffraction and energy-dispersive spectroscopy (EDS) were performed by means of a JEOL 2010 transmission electron microscope equipped with an INCA analyzer. The iodometric titration method was applied to determine the average formal oxidation state of cobalt species. Each sample (ca. 50 mg) was dissolved in a molar acetic buffer solution (ca. 50 mL) containing an excess of KI (ca. 1 g). Co(+III) and Co(+IV) species are reduced to Co(+II) together with formation of iodine species in a stoichiometric amount. Iodine is then titrated with a $Na_2S_2O_3$ 0.1 N solution using Thiodene (starch) as a colorimetric indicator. Powder neutron diffraction data were collected on the PUS diffractometer at the JEEP II reactor in Kjeller with a wavelength of 1.5554 Å generated from a Ge (511) reflection monochromator. The fullprof program,[32] included in the winplotr package,[33] was used for Rietveld refinements.

Resistivity (ρ) measurements were based on the four-probe technique with ultrasonically deposited indium contacts. The T-dependent ρ data were collected both under a magnetic field of 0 and 7 T on a Quantum Design physical properties measurement system (PPMS). Magnetic susceptibility was obtained by dividing the magnetization (M) by the magnetic field (0.3 T) with M data collected in zero-field-cooling and field-cooling mode with a SQUID magnetometer (MPMS, Quantum Design).

RESULTS AND DISCUSSION

1. Preliminary Structural Analyses. The as-synthesized material was first analyzed by powder X-ray diffraction, showing a low angular peak corresponding to a primitive d spacing close to 14 Å. Electron diffraction was performed, and the reciprocal space was reconstructed by tilting around this long axis, resulting in a unit cell of $a_p \times a_p \times 28$ Å (a_p being the cell parameter of the cubic perovskite structure) with the reflection conditions hkl: $h + k + l = 2n$, no supplementary condition being observed. The most symmetric space group $I4/mmm$ was retained and allowed to index the aforementioned powder X-ray diffraction pattern. In parallel, EDS experiments were carried out on the sample, yielding determination of a $Sr_{3.23(10)}La_{0.77(10)}Co_{2.86(9)}$ cationic composition, in good agreement with the nominal content $Sr_{3.30}La_{0.70}Co_{2.75}$. At this stage and given the composition the unit cell could be seen as characteristic of an RP3 structure. According to the synthetic conditions, a slight Co deficiency is found in the material when compared to a theoritical RP3 ($A_4B_3O_{10}$), suggesting that carbonates are incorporated in the structure and partially substitute the B-site element. A similar mechanism was reported in a Fe oxycarbonate,[34] while we recently discussed

dx.doi.org/10.1021/ic3017694 | Inorg. Chem. 2013, 52, 1265−1274

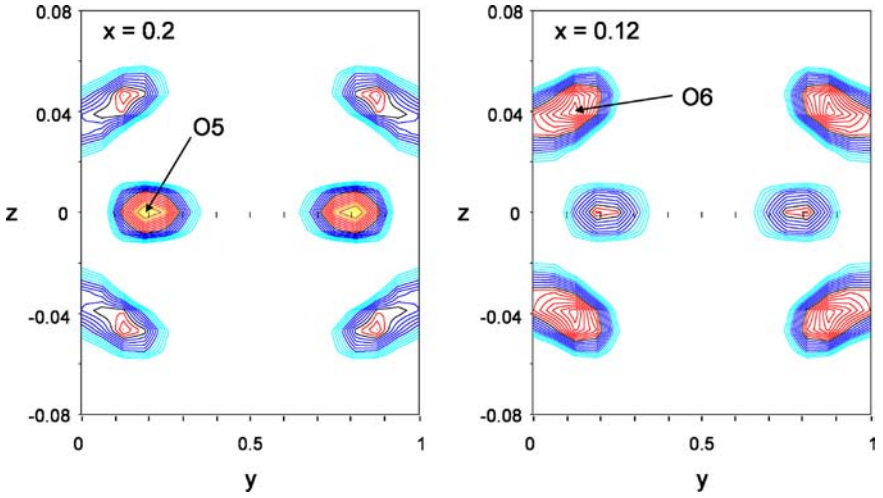

Figure 2. Selected portions of Fourier difference maps on two sections of the unit cell showing scattering densities at approximately 1.2 Å of (0 0 0).

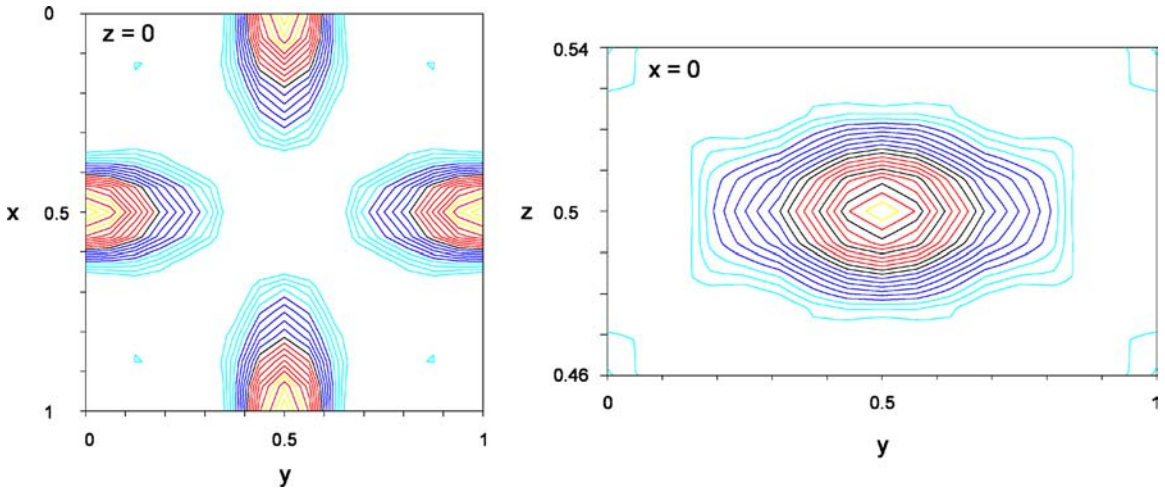

Figure 3. Fourier difference maps showing a large, anisotropic delocalization of scattering density around (0 0.5 0).

the mechanism of partial substitution in cobaltates in a related RP3 derivate.[31] Information on Co valence was collected by the mean of iodometric titrations, yielding a formal oxidation state of $Co^{+2.45(5)}$ in the present phase. Combining this latter technique with EDS an analytical chemical formula of $Sr_{3.23}La_{0.77}Co_{2.86}(CO_3)_{0.14}O_{7.75(15)}$ is proposed, showing good agreement with the nominal composition $Sr_{3.30}La_{0.70}Co_{2.75}(CO_3)_{0.25}O_{7.77}$. Such a formula involves a large amount of oxygen vacancies when compared to the theoretical $A_4B_{3-x}(CO_3)_xO_{10-4x}$ formula with $x = 0.25$.

As a large anion deficiency was suggested in the as-synthesized material, its potential for incorporating larger oxygen content was studied by the mean of postsynthesis annealing. Powder X-ray diffraction data collected on a sample annealed at 400 °C under an O_2 pressure (P_{O_2}) of 10 MPa showed a shift of diffraction peaks toward lower 2θ angles correlated with a significant variation of the relative intensities (Figure 1). Iodometric titrations showed an oxidation of cobalt within the sample with an average formal valence state of 3.15(5), compared to 2.45(5) before treatment under P_{O_2}. EDS and electron diffraction analyses showed, respectively, that the cationic composition and existence conditions were unchanged. The PXD pattern could be fully indexed with space group *I*4/*mmm* in a unit cell of reduced volume compared to the as-made sample, in agreement with the decrease of the average ionic radii from Co^{2+}/Co^{3+} to Co^{3+}/Co^{4+} species.

In order to study carbonate incorporation as well as locate the remarkable effects of oxygen deficiency a powder neutron diffraction study was carried out on 5 g samples. This work was performed on the as-synthesized and P_{O_2} annealed samples.

2. Neutron Diffraction Study. Given the nature of the effects to be searched, the approach of a progressive construction of the final model was chosen. Therefore, no carbonate nor oxygen deficiency was introduced in the starting model, and atomic coordinates of a "stoichiometric" RP3 $Sr_{3.23}La_{0.77}Co_3O_{10}$ (considering Sr and La similar neutron scattering lengths, the Sr/La ratio deduced from EDS analyzes was retained for setting the A-site composition) were first refined, yielding convergence with the reliability factors R_p = 33.5%, χ^2 = 8.37, R_{Bragg} = 24.60%. These reliability factors were then lowered to R_p = 19.8%, χ^2 = 2.30, R_{Bragg} = 11.25% by taking into account the oxygen deficiency. Refining isotropic thermal parameters resulted in abnormally high values observed in the central perovskite layers for O(2) and O(4) (up to 30 $Å^2$ for the latter), while the Co(1) position was associated to a negative number (Figure 2). Structural determination was clearly affected by the presence of carbonate, and Fourier difference maps analysis was performed. Scattering centers

dx.doi.org/10.1021/ic3017694 | *Inorg. Chem.* 2013, 52, 1265−1274

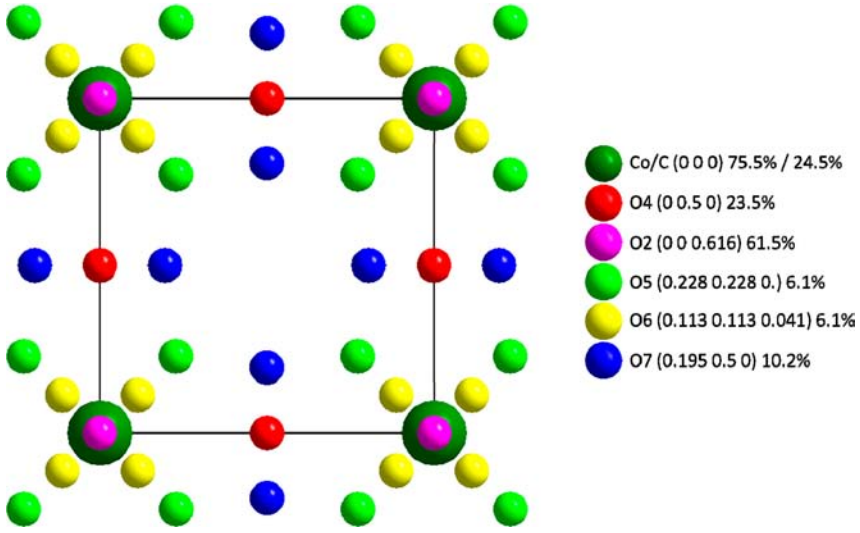

Figure 4. View along [001] of the disorder introduced in the central perovskite block of the RP3 due to combination of carbonation and high oxygen deficiency. Occupancies and fractional coordinates from the final refinement are quoted.

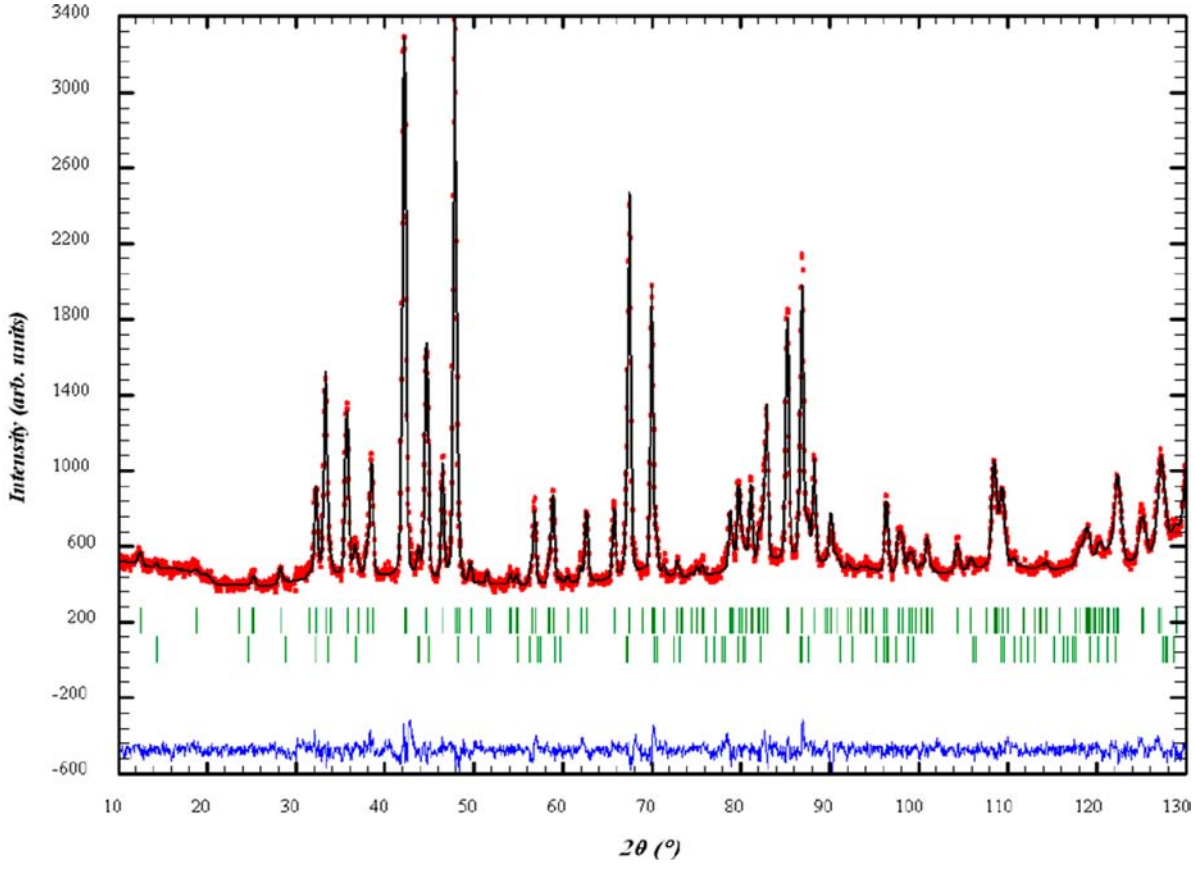

Figure 5. Rietveld analysis of powder neutron diffraction data: final observed (red), calculated (black), and difference (blue) diagrams for $Sr_{3.23}La_{0.77}Co_{2.755(15)}(CO_3)_{0.245(15)}O_{7.65(17)}$. Secondary phase consists of (La,Sr)CoO_x perovskite (3%).

associated to two distinct crystallographic sites could be detected in the central perovskite unit at approximate positions (0.2, 0.2, 0) and (0.1, 0.1, 0.4). Two triangles with (0 0 0) as a gravity center are formed by these two sites, leading to distances of 1.2 Å, which were assigned to C−O bonds in a carbonate group located on (0 0 0). A mixed Co(1)/C site associated to two extra oxygen sites O(5) and O(6) was considered for the following steps. Given the location on high-multiplicity sites with extremely low occupancies, proportionality was applied when refining occupancies within the carbonate, coordinating one C atom to one O(5) and two O(6), in order to respect the reasonable assumption of a CO_3 stoichiometry for each carbonate group. The O(4) thermal parameter remained excessively large after carbonate introduction with a refined value close to 10 $Å^2$. Refining anisotropic thermal parameters yielded an abnormally high β_{11} parameter

dx.doi.org/10.1021/ic3017694 | Inorg. Chem. 2013, 52, 1265−1274

corresponding to a mean square displacement of 0.6 Å, suggesting a split site. Another set of Fourier difference maps was therefore calculated with an O(4) occupancy fixed to zero, leading to observation of a diffuse scattering density on the basal plane map for $z = 0$. While a splitting model around the original 4c site would be suggested by the noticeable anisotropy of the scattering, this feature is however centered on the original *4c* site, located on (0, 0.5, 0) (Figure 3). When refined, the splitted site alone was therefore not sufficient to assess the oxygen repartition around (0, 0.5, 0), still leading to a high value of the thermal parameter (8 Å^2), while a positive scattering centered on *4c* remained on Fourier difference maps calculated after this step. Thus, a new *4c* oxygen position was added and the scattering delocalization was modeled with 2 sites on O(4) (0, 0.5, 0) and O(7) (x, 0.5, 0), resulting in lowered thermal parameters for the concerned atoms. This model fits well the Fourier difference maps. Such a duality of the oxygen positions is also observed in the highly oxygen-deficient $Sr_3LaCo_{1.5}Fe_{1.5}O_{7.5}$,[35] showing a split site combined with a residual occupancy on *4c*. A problem arising from this high degree of disorder in the central perovskite block (combination of the O(7) split site, carbonation, and nonnegligible occupancy on O(4)) was the extreme proximity of anionic sites (several distances lesser than 1 Å) in the concerned layers coupled with the low occupancies on the high-multiplicity site (Figure 4). Given the interplay between site locations, fractional occupancies, and thermal parameters, the poor scattering definition resulting from such proximity, and weak occupancies on the sites, one degree of freedom was suppressed: thermal parameters of these 4 sites were not fixed but constrained to be equal during the refinement cycles to avoid the "shadowing" of an oxygen site by another. Refinement of the Sr/La repartition showed no clear ordering, and the respective fractions occupying the two distinct A sites are almost equal within standard deviation ranges. Final reliability factors were R_p = 3.55%, R_{wp} = 4.61%, χ^2 = 1.28, R_{Bragg} = 3.80% for a model leading to the chemical formula $Sr_{3.23}La_{0.77}Co_{2.755(15)}(CO_3)_{0.245(15)}O_{7.65(17)}$. Experimental, calculated, and difference curves are presented in Figure 5, while the structural model is depicted in Figure 6. Structural parameters and principal interatomic distances are summarized in Tables 1 and 2, respectively.

Evolution of the material after postsynthesis annealing was studied by neutron diffraction in order to locate oxygen incorporation in the structure by means of Rietveld refinements (Figure 7). The same refinement procedure as for the as-synthesized material was applied with a few noticeable differences concerning the central perovskite layers: no splitting around the 4c site was observed; therefore, these layers contain a reduced number of crystallographic sites (no O(7)) with greater occupancies of O(3) and O(4), resulting in a better definition of the scattering densities that allows one to refine all atomic parameters independently, except for O(5) and O(6) (both composing the carbonate groups), for which extremely short distances and weak occupancies remain, causing the constraint of thermal parameters to be equal during refinement. Final reliability factors for this refinement were R_p = 3.40%, R_{wp} = 4.43%, χ^2 = 1.88, R_{Bragg} = 3.80% for a model leading to the chemical formula $Sr_{3.23}La_{0.77}Co_{2.81(1)}(CO_3)_{0.19(1)}O_{8.97(11)}$. Structural parameters and principal interatomic distances are summarized in Tables 3 and 4, respectively.

3. Structural Discussion. This compound can be seen as an oxygen-deficient RP3 member, with vacancies mainly

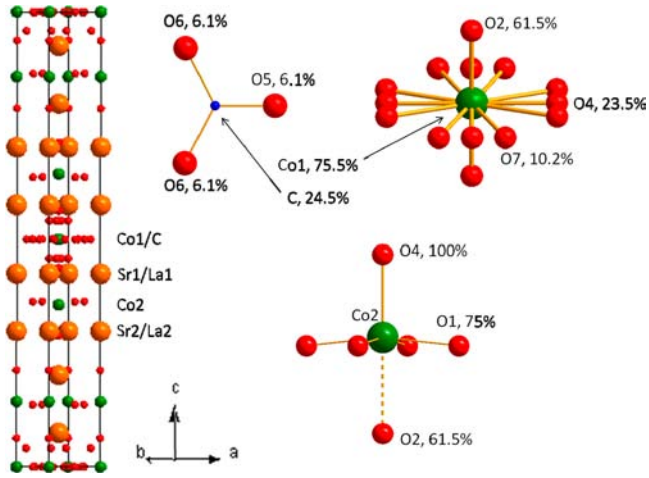

Figure 6. structural model for $Sr_{3.23}La_{0.77}Co_{2.755(15)}(CO_3)_{0.245(15)}O_{7.65(17)}$ and cobalt and carbon environments in the structure. Corresponding colors: La/Sr (orange), Co (green), C (blue), and O (red).

present in the central perovskite block, combined with a disordered carbonation on this same block, by substitution of CO_3 triangles for CoO_x polyedra. For consistency with parameters extracted from the Rietveld refinements, quoted for the forthcoming structural description, we will retain a chemical formula determined by combination of EDS and powder neutron diffraction analysis, namely, $Sr_{3.23}La_{0.77}Co_{2.755(15)}(CO_3)_{0.245(15)}O_{7.65(17)}$ was retained. The large anionic deficiency does not result in a distortion of the crystallographic unit cell, as can be seen in numerous perovskites or Ruddlesden−Popper derivate structures. The mixed character $(La,Sr)Co_{0.755}O_{2.11}/(CO_3)_{0.245}$ of the central perovskite block prevents any long-range vacancy ordering with carbonates taking multiple orientations. This most probably results in multiple orientations for the Co polyhedra in order to minimize O−O repulsions with disordered CO_3 groups coexisting within the same layer, the *I4/mmm* symmetry being retained despite a large deviation to the ideal O_{10} stoichiometry. Refinement of the Sr/La repartition also showed no clear ordering, and the respective fractions occupying the two distinct A sites are almost equal within standard deviation ranges. A split site model had to be taken into account in order to model the oxygen repartition in the central perovkite block; this is accompanied by an extremely short Co(1)−O(2) of 1.793(11)Å distance, in opposition to an extremely long Co(2)−O(2) distance of 2.313 Å. To gain a better understanding of these conjugated features, it is essential to put them in context of other oxygen-deficient RP3 members where the central perovskite block is altered by the anion vacancies (Table 5). As oxygen deficiency occurs in these compounds, the transition metal average coordination number in the central perovkite block is less than 6 and not integer meaning several types of polyedra coexist with an apparent disorder (*I4/mmm* symmetry) in the same perovskite block. In parallel, as oxygen content decreases from $LaSr_3Fe_3O_{9.88}$ to $LaSr_3(Fe_{0.8}Al_{0.2})_3O_{8.95}$,[47] the thermal displacement of O4 increases from 0.92 to 4.7 Å^2. The physical meaning of this B increase can be seen as the increase of positional disorder due to the coexistence of MO_{6-x} polyedra such as MO_5 square-based pyramids or MO_4 tetraedra. To retain the transition metal in the neighboring anions center of gravity, the defect

dx.doi.org/10.1021/ic3017694 | Inorg. Chem. 2013, 52, 1265−1274

Table 1. Refined Structural Parameters for $Sr_{3.23}La_{0.77}Co_{2.755(15)}(CO_3)_{0.245(15)}O_{7.65(17)}$[a]

atom	site	x	y	z	B_{iso} (Å^2)	n
Sr1/La1	4e	0	0	0.5747(2)	1.73(11)	2.99/1.01(22)
Sr2/La2	4e	0	0	0.70176(11)	0.82(9)	3.47/0.53(22)
Co1/C	2a	0	0	0	1.7(3)	1.51/0.49(3)
Co2	4e	0	0	0.1429(3)	0.1(2)	4
O1	8j	0	0.5	0.13642(16)	1.35(8)	7.07(7)
O2	4e	0	0	0.0616(4)	3.2(4)[c]	2.46(10)
O3	4e	0	0	0.21215(17)	0.73(7)	4[b]
O4	4c	0	0.5	0	3.2(4)[c]	0.94(8)
O5	8h	0.228(6)	0.228(6)	0	3.2(4)[c]	0.49(3)
O6	16m	0.113(3)	0.113(3)	0.041(3)	3.2(4)[c]	0.98(6)
O7	8j	0.195(12)	0.5	0	3.2(4)[c]	0.82(9)

[a] $I4/mmm$; a = 3.8400(1) Å; c = 28.692(2) Å. [b] 3.97(6) when refined. [c] Constrained to be equal due to extreme proximity of oxygen sites in the layer (see Results and discussion).

Table 2. Principal Interatomic Distances in $Sr_{3.23}La_{0.77}Co_{2.755(15)}(CO_3)_{0.245(15)}O_{7.65(17)}$

M−O	d (Å)	× n	M−O	d (Å)	× n
Sr/La(1)−O(1)	2.604(3)	× 3.535	Co(1)−O(2)	1.793(11)	× 1.63
Sr/La(1)−O(2)	2.7377(15)	× 2.46	Co(1)−O(4)	1.9200	× 1.245
Sr/La(1)−O(4)	2.878(3)	× 0.94	Co(1)−O(7)	2.06(4)	× 0.47
Sr/La(1)−O(5)	2.603(13)	× 0.245			
Sr/La(1)−O(6)	2.95(3)	× 0.49	Co(2)−O(1)	1.9307(10)	× 3.5
Sr/La(1)−O(6)	2.33(3)	× 0.245	Co(2)−O(2)	2.313(14)	× 0.65
Sr/La(1)−O(7)	2.44(2)	× 0.82	Co(2)−O(3)	1.986(9)	× 1
			Co(2)−O(6)	3.08(4)	× 0.19
Sr/La(2)−O(1)	2.692(3)	× 3.535			
Sr/La(2)−O(3)	2.7321(5)	× 4	C−O(5)	1.24(2)	× 1
Sr/La(2)−O(3)	2.465(5)	× 1	C−O(6)	1.33(5)	× 2

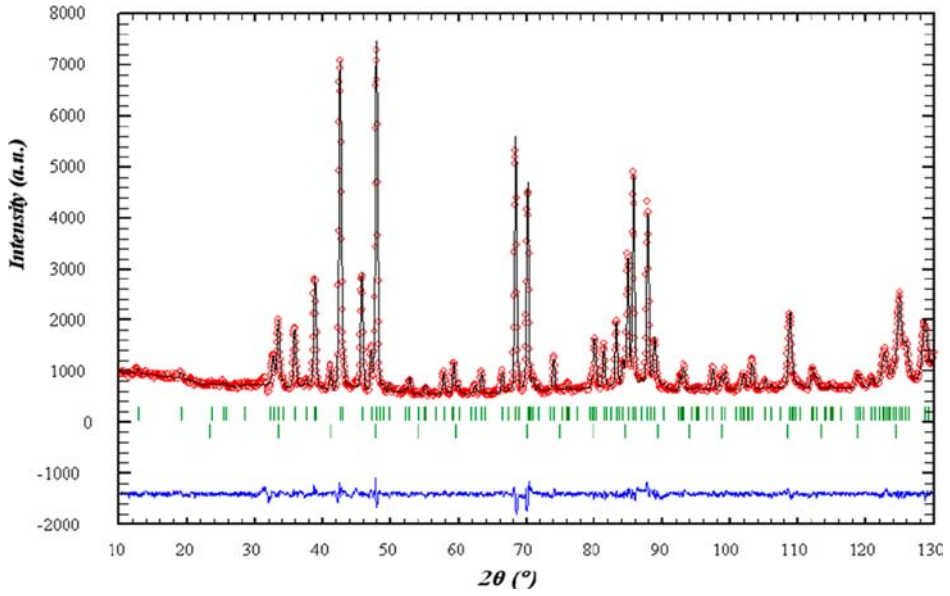

Figure 7. Rietveld analysis of powder neutron diffraction data collected after annealing under P_{O_2} = 10 MPa: final observed (red), calculated (black), and difference (blue) diagrams for $Sr_{3.23}La_{0.77}Co_{2.81(1)}(CO_3)_{0.19(1)}O_{8.97(11)}$. Secondary phase consists of $LaSrCoO_4$ (2%).

structure tends to the split site model upon introduction of MO_5 or MO_4 polyedra, inducing delocalization of neutron scattering density from the 4c site. With further reduction of the coordination number in the central perovskite block, splitting of the O4 site can be taken into account to model the scattering density around the 4c site by powder diffraction analysis, as in the present $Sr_{3.23}La_{0.77}Co_{2.755(15)}(CO_3)_{0.245(15)}O_{7.65(17)}$ or $LaSr_3Co_{1.5}Fe_{1.5}O_{7.5}$.[35] Adding to the large oxygen deficiency, an increased apical bonding is required to compensate for the low in-plane coordination number of Co(1), leading to the extremely short Co(1)−O(2) distance. As a result of the increase in Co(1)−O(2) bonding, Co(2)−O(2) bonding is reciprocally decreased, yielding larger Co(2)−O(2) interatomic distances as the oxygen content is lowered,

dx.doi.org/10.1021/ic3017694 | Inorg. Chem. 2013, 52, 1265−1274

Table 3. Refined Structural Parameters for the Oxidized $Sr_{3.23}La_{0.77}Co_{2.81(1)}(CO_3)_{0.19(1)}O_{8.97(11)}$[a]

atom	site	x	y	z	B_{iso} (Å^2)	n
Sr1/La1	4e	0	0	0.57027(11)	0.85(2)	3.11/0.89(24)
Sr2/La2	4e	0	0	0.70077(12)	0.31(9)	3.35/0.65(24)
Co1/C	2a	0	0	0	0.64(17)	1.64/0.36(3)
Co2	4e	0	0	0.1412(3)	0.45(11)	4
O1	8j	0	0.5	0.13797(10)	0.61(4)	8
O2	4e	0	0	0.06748(22)	0.98(14)	3.17(8)
O3	4e	0	0	0.21138(12)	1.15(8)	4
O4	4c	0	0.5	0	3.38(23)	2.90(5)
O5	8h	0.216(4)	0.216(4)	0	2.1(8)[b]	0.36(3)
O6	16m	0.087(4)	0.087(4)	0.041(3)	2.1(8)[b]	0.72(6)

[a] $I4/mmm$; a = 3.83187(8) Å; c = 28.0582(7) Å. [b] Constrained to be equal due to extreme proximity of oxygen sites in the layer (see Results and Discussion).

Table 4. Principal Interatomic Distances in the Oxidized $Sr_{3.23}La_{0.77}Co_{2.81(1)}(CO_3)_{0.19(1)}O_{8.97(11)}$

M−O	d (Å)	× n	M−O	d (Å)	× n
Sr/La(1)−O(1)	2.698(3)	× 4	Co(1)−O(2)	1.894(6)	× 1.933
Sr/La(1)−O(2)	2.71066(18)	× 3.17	Co(1)−O(4)	1.9159	× 3.537
Sr/La(1)−O(4)	2.749(2)	× 2.90			
Sr/La(1)−O(5)	2.36(3)	× 0.18	Co(2)−O(1)	1.9181(3)	× 4
Sr/La(1)−O(6)	2.82(3)	× 0.36	Co(2)−O(2)	2.068(8)	× 0.79
Sr/La(1)−O(6)	2.44(3)	× 0.18	Co(2)−O(3)	1.969(7)	× 1
			Co(2)−O(6)	2.69(4)	× 0.19
Sr/La(2)−O(1)	2.465(3)	× 4			
Sr/La(2)−O(3)	2.7258(4)	× 4	C−O(5)	1.27(2)	× 1
Sr/La(2)−O(3)	2.6030(19)	× 1	C−O(6)	1.35(5)	× 2

reaching 2.41 Å in $LaSr_3Co_{1.5}Fe_{1.5}O_{7.5}$.[35] This weakening of one of the apical bonds can be compensated by the larger coordination number for Co(2).

The as-synthesized material can be seen as an oxygen-deficient RP3 member. For consistency between structural analysis and structural discussion, chemical formula determined by combination of EDS and powder neutron diffraction analysis, namely, $Sr_{3.23}La_{0.77}Co_{2.755(15)}(CO_3)_{0.245(15)}O_{7.65(17)}$, was retained. The oxygen deficiency mainly takes place in the central perovskite block of the RP3 and does not result in a crystallographic distortion of the unit cell. Several factors combine to prevent long-range ordering of oxygen vacancies: quench from high temperature, noninteger oxygen content, and partial introduction of carbonates yielding, for example, a central perovskite block with $(La,Sr)Co_{0.755}O_{2.11}/(CO_3)_{0.245}$ composition.

Co(2) average coordination number is 4.54 without taking into account O(2) in the coordination sphere due to $d_{Co(2)-O(2)}$ = 2.313 Å. Co(2) environment is therefore composed of 46% tetrahedral CoO_4 and 54% square-based pyramidal CoO_5, both being very similar to those reported in the H_2 reduced RP2 phase $Sr_3FeCoO_{7-\delta}$ (δ = 1.55), in terms of bond distances and angles.[36] The average coordination number of Co(1) is 3.96, indicating a tetrahedral environment. From the fractional occupancies of concerned oxygen sites, two distinct types of CoO_4 tetrahedra are formed with two different orientations and a highly distorted geometry, as observed in other perovskite derivates combining this environment with a large oxygen deficiency.[36−38] The CO_3 groups show a regular triangular planar configuration with C−O(5) and C−O(6) distances of 1.24 and 1.33 Å and O(5)−C−O(6) and O(6)−C−O(6) bond angles of 117(4)° and 125(7)°, respectively.

The variety of Co−O bond lengths from one layer to another is remarkable. To put this in context, Table 5 shows the structural influence of oxygen deficiency in several (structurally comparable) Fe-rich RP3 compounds. From $LaSr_3M_3O_{9.88}$[47] to $LaSr_3M_3O_{7.5}$[35] an apparent vacancy disorder is retained ($I4/mmm$ symmetry), and M(1)−O(2) and M(2)−O(2) distances, respectively, evolve from 1.935 to 1.786 Å and 1.968 to 2.411 Å. Shortening of M(1)−O(2) occurs to compensate the low in-plane coordination number by stronger apical bonding, and M(2)−O(2) is reciprocally elongated. One also notes the increase of the O(4) thermal displacement parameter with

Table 5. Selected Structural Parameters Affected by the Oxygen Deficiency in the Central Perovskite Block of Various RP3 Compounds

compound	M (1)[b] average coordination number	B_{eq}(O4) (Å^2)	d M(1)−O(2) (Å)	d M(2)−O(2) (Å)	ref
$LaSr_3Fe_3O_{9.88}$	5.82	0.92	1.935	1.968	47
$LaSr_3(Fe_{0.86}Al_{0.14})_3O_{9.28}$	5.00	2.4	1.889	2.063	47
$LaSr_3Fe_3O_{9.45}$	5.06	3.1	1.857	2.129	47
$LaSr_3(Fe_{0.85}Al_{0.15})_3O_{9.05}$	4.6	3.9	1.854	2.144	47
$LaSr_3(Fe_{0.8}Al_{0.2})_3O_{8.95}$	4.58	4.7	1.879	2.097	47
$LaSr_3Fe_{1.5}Co_{1.5}O_{7.5}$[a]	3.18	1.18	1.786	2.411	35
$Sr_{3.23}La_{0.77}Co_{2.81}(CO_3)_{0.19}O_{8.97}$	5.47	3.38	1.894	2.068	this work
$Sr_{3.23}La_{0.77}Co_{2.755}(CO_3)_{0.245}O_{7.65}$[a]	3.96	3.2	1.793	2.313	this work

[a] Splitted site model. [b] In the central layer of the perovskite block.

dx.doi.org/10.1021/ic3017694 | Inorg. Chem. 2013, 52, 1265−1274

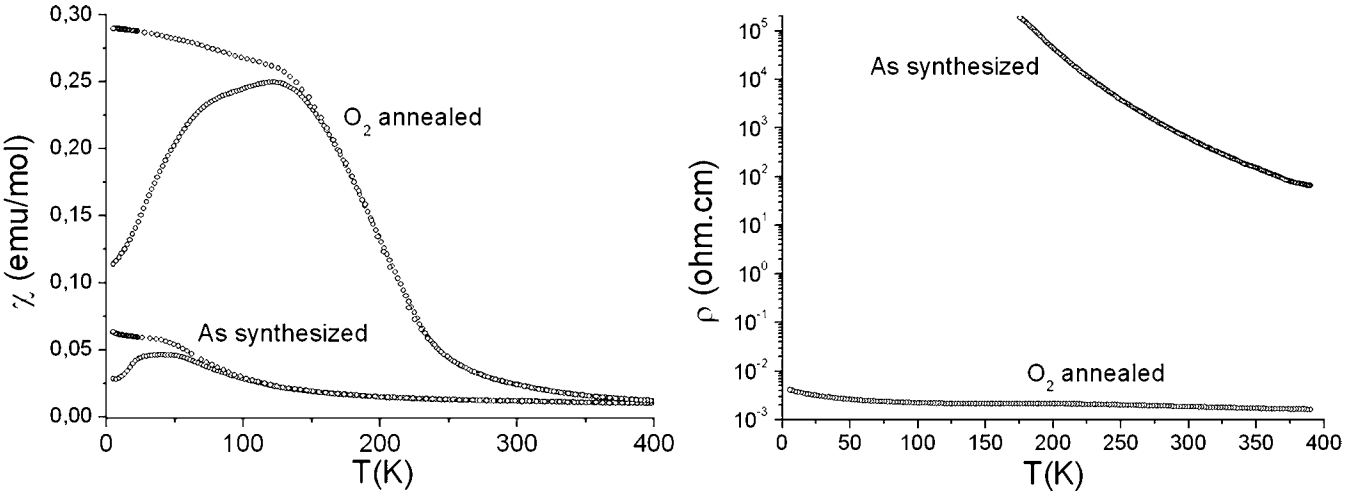

Figure 8. Evolution of magnetotransport properties evolution from the as-synthesized to the 10 MPa P_{O_2} annealed samples: (left) magnetic susceptibility; (right) resistivity.

oxygen deficiency until a split site is effective. This most probably translates the increase of positional disorder as several types of polyhedra coexist in the central perovskite block rather than an actual dynamic displacement. Note that relatively large thermal displacement parameters can also be observed in parent oxygen-deficient perovskites such as the layered $Sr_{0.7}Y_{0.3}CoO_{2.65-\delta}$ where a mixed cobalt environment in the oxygen-deficient layers results in an isotropic thermal factor of 5.2(4) for equatorial oxygen atoms compared to 0.54(5) for the equatorial oxygen-filled sites.[39] Table 5 shows that the structural behavior of the as-synthesized $Sr_{3.23}La_{0.77}Co_{2.755(15)}(CO_3)_{0.245(15)}O_{7.65(17)}$ (and of the oxidized $Sr_{3.23}La_{0.77}Co_{2.81(1)}(CO_3)_{0.19(1)}O_{8.97(11)}$) fits qualitatively well with the evolution observed in these analogue Fe-rich RP3 compounds.

The oxidized $Sr_{3.23}La_{0.77}Co_{2.81(1)}(CO_3)_{0.19(1)}O_{8.97(11)}$ can also be seen as an RP3 member with the same disordered carbonation taking place in the central layer of the perovskite block. However, though anion deficiency is still present, its oxygen content has been dramatically increased by the annealing under P_{O_2}. For the same reasons discussed when dealing with the as-made material, the chemical formula we retain here is the one combining EDS and PND, yielding $Sr_{3.23}La_{0.77}Co_{2.81(1)}(CO_3)_{0.19(1)}O_{8.97(11)}$. The carbonation rate from the as-made to the oxidized compound is retrieved by powder neutron diffraction analysis in an interval containing three standard deviations and therefore shows good agreement between the two sets of refinements, especially given the small fraction of carbon substituted for cobalt—carbon having the largest scattering length of both elements. The increase of oxygen content observed after annealing is calculated to be 1.32 oxygens per RP3 formula unit. The central perovskite block is drastically affected by oxygenation. No splitting around O(4) is observed, and O(2) and O(4) fractional occupancies rise, respectively, from 0.615 and 0.235 to 0.803 and 0.722. A filling of the O(1) site in the external layer of the perovskite block also occurs, which results in full occupancy compared to the previously determined 0.884. Cobalt environments have their coordination numbers elevated by P_{O_2} treatment, resulting in average $Co(1)O_{5.55}$ and $Co(2)O_{5.76}$ polyhedra. Co(1) environment is therefore a mixture of 55% CoO_6 octahedra and 45% CoO_5 square-based pyramids having their basis parallel to the *c* axis of the unit cell. Co(2) environment shows a dominant octahedral configuration (76%) mixed with square-based pyramids (24%) with basis perpendicular to the *c* axis due to a small amount of vacancies on O(2) and O(3) positions. For its largest fraction the pyramidal environment of Co(2) is imposed by carbonation, which implies an O(3) vacancy due to the presence of O(6) to coordinate the carbon (O(3)−O(6) distance would otherwise be shorter than 1 Å). Therefore, the 24% pyramids for Co(2) and 21% carbon in the central perovskite block are in good agreement with the partial occupancy of 0.803 for O(3) site that has reached its maximum potential for oxygenation upon P_{O_2} annealing given the presence of 0.0475 from the CO_3 groups that cannot coexist in directly neighboring sites.

The product of the oxidizing treatment is $Sr_{3.23}La_{0.77}Co_{2.81(1)}(CO_3)_{0.19(1)}O_{8.97(11)}$. Its oxygen content is dramatically increased, and the carbonation rate from the as-made to the oxidized compound is retrieved by powder neutron diffraction analysis in an interval containing three standard deviations, therefore showing good agreement between the two sets of refinements, especially given the small fraction of carbon substituted for cobalt. The increase of oxygen content observed after annealing is calculated to be 1.32 oxygens per RP3 formula unit. The central perovskite block is drastically affected by oxygenation. The splitting around O(4) is no longer observed, and filling of vacancies mainly occurs on the O(2) and O(4) sites. Filling of the O(1) site in the external layer of the perovskite block also occurs, which results in full occupancy. Co(1) environment is then a mixture of 55% CoO_6 octahedra and 45% CoO_5 square-based pyramids having their basis parallel to the *c* axis of the unit cell. The Co(2) environment shows a dominant octahedral configuration (76%) mixed with square-based pyramids (24%), with basis perpendicular to the *c* axis due to a small amount of vacancies on the O(2) position. The 24% square-based pyramidal Co(2) correlates well with the 19% of carbonates in the central perovskite block, which implies a maximal occupancy of 0.82 for O(2) (0.79 here).

4. Physical Properties as a Function of Oxygen Nonstoichiometry. A dramatic evolution of magnetotransport properties is observed in the system subject to oxygen content evolution (Figure 8). Indeed, the magnetic susceptibility of the as-made $Sr_{3.23}La_{0.77}Co_{2.755(15)}(CO_3)_{0.245(15)}O_{7.65(17)}$

dx.doi.org/10.1021/ic3017694 | Inorg. Chem. 2013, 52, 1265−1274

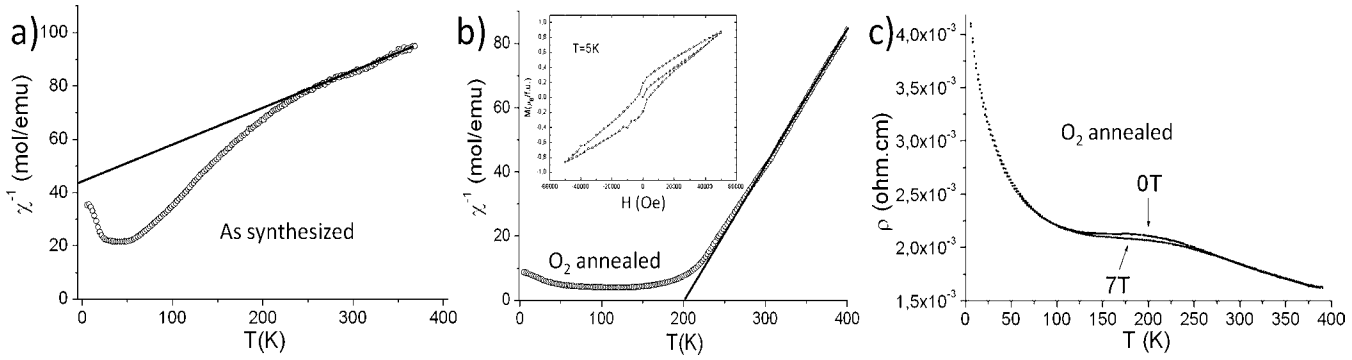

Figure 9. (a) Inverse magnetic susceptibility as a function of temperature for the as-synthesized material $Sr_{3.23}La_{0.77}Co_{2.755(15)}(CO_3)_{0.245(15)}O_{7.65(17)}$. (b) Inverse magnetic susceptibility as a function of temperature for the oxidized material $Sr_{3.23}La_{0.77}Co_{2.81(1)}(CO_3)_{0.19(1)}O_{8.97(11)}$. (c) Resistivity of the oxidized material as a function of temperature at 0 and 7 T.

(Figure 8a) shows a transition with a peak at 40 K and a divergence of FC and ZFC curves below 100 K, resulting from a weak ferromagnetic contribution. The inverse susceptibility shows a linear regime that could be extrapolated according to the Curie–Weiss law (Figure 9b), leading to θ_p = −303 K, indicating the predominance of antiferromagnetic interactions in the paramagnetic state, due to Co^{2+}–O–Co^{3+} superexchange. Such configuration yields a semiconducting behavior with a low electronic conductivity (Figure 9c). In parallel, the magnetic susceptibility of the oxidized $Sr_{3.23}La_{0.77}Co_{2.81(1)}(CO_3)_{0.19(1)}O_{8.97(11)}$ shows a large peak at 125 K with a divergence of the FC and ZFC curve below 150 K (Figure 8a). Upon the change from Co^{2+}–O–Co^{3+} to Co^{3+}–O–Co^{4+} superexchange one can expect ferromagnetic interactions to become dominant in the paramagnetic regime as exemplified by θ_p = 203 K deduced from a Curie–Weiss law fitting above 250 K (Figure 9b). This contribution is also nonnegligible in the ordered state, as shown by the hysteresis loop on the $M = f(H)$ graph (Figure 9b inset). This ferromagnetic contribution favors electron delocalization, leading to a decrease of the electronic resistivity by 5 orders of magnitude when compared to the as-made material ($\rho_{300K} \approx$ 500 Ω·cm and $\rho_{300K} \approx$ 2 mΩ·cm for the as-made and oxidized sample, respectively). In addition, in the magnetic transition temperature domain the resistivity is sensitive to application of magnetic field and a negative magnetoresistance reaching −2.5% at 187 K under 7 T is observed, comparable to other Co^{3+}–O–Co^{4+} mixed-valent compounds such as $SrCoO_{3-\delta}$ [42] or $Sr_{2.75}Ce_{0.25}Co_2O_{6.7}$.[43]

CONCLUDING REMARKS

Here we report the complex $Sr_{3.23}La_{0.77}Co_{2.755}(CO_3)_{0.245}O_{7.65}$ oxide, related to the n = 3 member of the RP series, stabilized by introduction of carbonate groups in the crystal structure via a suitable synthetic method. Clearly, $Sr_{3.23}La_{0.77}Co_{2.755(15)}(CO_3)_{0.245(15)}O_{7.65(17)}$ is highly disordered oxygen deficient with no ordering of the O vacancies or in the mixed Co/C site. However, it is worth noting that carbonation occurs only in a specific block of the structure, while the anion deficiency shows a strong preferential repartition in this same block. Interestingly, carbonates have a stabilizing effect on the RP3-type framework, since all attempts to synthesize the carbonate-free RP3 cobaltite have failed. Given the crystal chemistry mechanism of carbonate incorporation in perovskite derivates,[40,41] odd terms of the RP series should allow the polyanions to be introduced while retaining a symmetrical stacking sequence, therefore favoring the RP3 framework upon the RP2 over the course of CO_3^{2-} reaction with other constituents of the mixture at high temperature in the sealed tube. Moreover, the combined effect of carbonation (which implies by crystal chemistry an oxygen impoverishment of the central perovskite block following the mode $A_4B_{3-x}(CO_3)_xO_{10-4x}$) and large nominal oxygen deficiency stabilizes an RP phase derivate with an extensively low average cobalt coordination number in the structure (4.35 when accounting for Co(2) and Co(1)), which is normally observed after highly reducing treatments only for comparable non-carbonated materials,[35−39] which frequently result in air-sensitive materials, which is not the case here. The present behavior results from an average cobalt oxidation state close to 2.54(5), i.e., greater than 2 even before P_{O_2} annealing (3.15(5) after P_{O_2}). Slight carbonation of perovskite derivates may therefore be a useful tool for obtaining uncommon transition metal environments in layered materials unreactive to ambient conditions.

Detailed study of the crystal chemistry of the as-made compound shows a large anionic deficiency in the framework which results in a large oxide ion uptake when annealed in a dioxygen-rich environment, yielding the obtention of $Sr_{3.23}La_{0.77}Co_{2.81}(CO_3)_{0.19}O_{8.97}$ with an average state valence close to +3.15. Magnetotransport properties are drastically affected by introduction of Co^{3+}–O–Co^{4+} superexchange upon postsynthesis oxidation, and both compounds exhibit extremely distinct behaviors. Previous articles report the difficulty in obtaining a Co-based RP3,[44] which could be systems with remarkable properties, notably in the field of technologies requiring mixed electron–ion conductivity (SOFC technology, gas-separating membranes, etc.). Here we should point out that Sr–Co-based perovskites have been extensively studied, leading to dominant materials in the aforementioned domains,[1,45,46] while RP structures have received considerably less attention, although they could be displaying similar properties. RP structures reduced thermal expansion when compared to their perovskites counterpart could also remove stability issues in multicomponent devices operating at HT. Owing to the stabilization by carbonation, we show that this Co-rich system displays a large range of oxygen nonstoichiometry when exposed to different conditions, allowing one to tune the magnetotransport properties and obtain a material with an electronic conductivity comparable to that of state of the art mixed conducting oxides. Moreover, obtaining $Sr_{3.23}La_{0.77}Co_{2.81}(CO_3)_{0.19}O_{8.97}$ at 400 °C proves that oxide

dx.doi.org/10.1021/ic3017694 | Inorg. Chem. 2013, 52, 1265−1274

anions are incorporated in the oxygen-deficient RP3 framework at moderate temperatures, showing that the system displays nonnegligible activity for catalysis of dioxygen molecule dissociation combined with important oxide anion bulk diffusivity. Therefore, RP3 compounds stabilized by carbonation display crystal chemical properties that make them attractive for generation of new relevant mixed conductors.

■ ASSOCIATED CONTENT

Supporting Information

Full powder CIF files for the as-synthesized and O_2 annealed materials are provided. This material is available free of charge via the Internet at http://pubs.acs.org.

■ AUTHOR INFORMATION

Corresponding Author

*E-mail: denis.pelloquin@ensicaen.fr.

Notes

The authors declare no competing financial interest.

■ ACKNOWLEDGMENTS

This work was carried out under the framework of the MADBLAST project supported by the ANR (Grant No. ANR-09-BLAN-0187-01). This work was supported by the FP7 European Initial Training Network SOPRANO (Grant No.GA-2008-214040).

■ REFERENCES

(1) Shao, Z.; Haile, S. M. *Nature* **2004**, *431*, 170.
(2) Dawber, M.; Rabe, K.; Scott. *J. Rev. Mod. Phys.* **2005**, *77*, 1083.
(3) Kim, C. H.; Qi, G.; Dahlberg, K.; Li, W. *Science* **2010**, *327*, 1624.
(4) Pena, M.; Fierro. *J. Chem. Rev.* **2001**, *101*, 1981.
(5) Jacobson, A. J. *Chem. Mater.* **2010**, *22*, 660.
(6) Fjellvag, H.; Guldbransen, E.; Aasland, S.; Olsen, A.; Hauback, B. *J. Solid State Chem.* **1996**, *124*, 190.
(7) Takada, K.; H. Sakurai, H.; Takyama-Mutomachi, E.; Izumi, F.; Dilanian, R. A.; Sasaki, T. *Nature* **2003**, *422*, 53.
(8) Orman, H. J.; Wiseman, P. J. *Acta Crystallogr. C* **1984**, *40*, 12.
(9) Bouwmeester, H. J. M.; Burgraaf, A. J. In *Fundamentals of Inorganic Membrane Science Technology*; Burgraaf, A. J., Cot, L., Eds.; Elsevier: Amsterdam, 1996; p 435.
(10) Tarancón, A.; Pena-Martinez, J.; Marrero-Lopez, D.; Morata, A.; Ruiz-Morales, J. C.; Nuñez, P. *Solid State Ionics* **2008**, *179*, 2372.
(11) Bednorz, J. G.; Müller, K. A. *Z. Phys. B* **1986**, *64* (1), 189.
(12) Von Helmolt, R.; Wecker, J.; Holzapfel, B.; Schultz, L.; Samwer, K. *Phys. Rev. Lett.* **1993**, *71*, 2331.
(13) Jin, S.; Tiefel, T. H.; McCormack, M.; Fastnacht, R. A.; Ramesh, R.; Chen, L. H. *Science* **1994**, *264*, 413.
(14) Hazen, R. M.; Prewitt, C. M.; Angel, R. J.; Ross, N. L.; Finger, L. W.; Hadidiacos, C. G.; Veblen, D. R.; Heaney, P. J.; Hor, P. H.; Meng, R. L.; Sun, Y. Y.; Wang, Y. Q.; Xue, Y. Y.; Huang, Z. J.; Gao, L.; Bechtold, J.; Chu, C. W. *Phys. Rev. Lett.* **1988**, *60*, 1174.
(15) Tarascon, J. M.; McKinnon, W. R.; Barboux, P.; Hwang, D. M.; Bagley, B. G.; Greene, L. H.; Hull, G. W.; Lepage, Y.; Stoffel, N.; Giroud, M. *Phys. Rev. B* **1988**, *38*, 8885.
(16) Sheng, Z. Z.; Hermann, A. M. *Nature* **1988**, *332*, 128.
(17) Dai, P.; Chakoumakos, B. C.; Sun, G. F.; Wong, K. W.; Xin, Y.; Lu, D. F. *Physica C* **1995**, *243*, 201.
(18) Ruddlesden, S. N.; Popper, P. *Acta Crystallogr.* **1958**, *11*, 58.
(19) Orera, A.; Slater, P. R. *Chem. Mater.* **2010**, *22*, 675.
(20) Dann, S. E.; Weller, M. T. *J. Solid State Chem.* **1995**, *115*, 499.
(21) Viciu, L.; Zandbergen, H. W.; Xu, Q.; Huang, Q.; Lee, M.; Cava, R. J. *J. Solid State Chem.* **2006**, *179*, 500.
(22) Hill, J. M.; Dabrowski, B.; Mitchell, J. F.; Jorgensen, J. D. *Phys. Rev. B* **2006**, *74*, 174417.
(23) Yamaura, K.; Huang, Q.; Cava, R. J. *J. Solid State Chem.* **1999**, *146*, 277.
(24) Gillie, L. J.; Hadermann, J.; Hervieu, M.; Maignan, A.; Martin, C. *Chem. Mater.* **2008**, *20*, 6231.
(25) Pelloquin, D.; Barrier, N.; Maignan, A.; Caignaert, V. *Solid State Sci.* **2005**, *7*, 853.
(26) Hansteen, O. H.; Fjellvag, H. *J. Solid State Chem.* **1998**, *141*, 212.
(27) Olafsen, A.; Fjellvag, H.; Hauback, B. C. *J. Solid State Chem.* **2000**, *151*, 46.
(28) Boulahya, K.; Parras, M.; Gonzalez-Calbet, J. M. *J. Solid State Chem.* **1999**, *145*, 116.
(29) Takami, T.; Ikuta, H.; Mizutani, U. *Jpn. J. Appl. Phys., Part1* **2004**, *43*, 8208.
(30) Sugiyama, J.; Nozaki, H.; Ikedo, Y.; Mukai, K.; Andreica, D.; Amato, A.; Brewer, J. H.; Ansaldo, E. J.; Morris, G. D.; Takami, T.; Ikuta, H. *JMMM* **2007**, *310*, 2719.
(31) Demont, A.; Pelloquin, D.; Hébert, S.; Bréard, Y.; Höwing, J.; Miyazaki, Y.; Maignan, A. *J. Solid State Chem.* **2011**, *184*, 1655.
(32) Rodriguez-Carvajal, J. *Physica B* **1993**, *192*, 55.
(33) Roisnel, T.; Rodriguez-Carvajal, J. *Materials Science Forum, Proceedings of the Seventh European Powder Diffraction Conference (EPDIC 7)*; Delhez, R.; Mittenmeijer, E. J., Eds.; Trans Tech Publications: Switzerland, 2000; pp 118−123.
(34) Breard, Y.; Michel, C.; Hervieu, M.; Raveau, B. *J. Mater. Chem.* **2000**, *10*, 1043.
(35) Bowman, A.; Allix, M.; Pelloquin, D.; Rosseinsky, M. J. *J. Am. Chem. Soc.* **2006**, *128*, 12606.
(36) Breard, Y.; Michel, C.; Hervieu, M.; Studer, F.; Maignan, A.; Raveau, B.; Mat, J. *Chem.* **2002**, *14*, 3128.
(37) Seddon, J.; Suard, E.; Mayward, M. A. *J. Am. Chem. Soc.* **2010**, *132*, 2802.
(38) Helps, R. M.; Rees, N. H.; Hayward, M. A. *Inorg. Chem.* **2010**, *49*, 11062.
(39) Li, Y.; Kim, Y. N.; Cheng, J. G.; Alonso, J. A.; Hu, Z. W.; Chin, Y. Y.; Takami, T.; Fernandez-Diaz, M. T.; Lin, H. J.; Chen, C. T.; Tjeng, L. H.; Manthiram, A.; Goodenough, J. B. *Chem. Mater.* **2011**, *23*, 5037.
(40) Breard, Y.; Michel, C.; Hervieu, M.; Nguyen, N.; Ducouret, A.; Hardy, V.; Maignan, A.; Raveau, B.; Bouree, F.; Andre, G. *Chem. Mater.* **2004**, *16*, 2895.
(41) Yamaura, K.; Huang, Q.; Lynn, J. W.; Erwin, R. W.; Cava, R. J. *J. Solid State Chem.* **2000**, *152*, 374.
(42) Bezdicka, P.; Wattiaux, A.; Grenier, J. C.; Pouchard, M.; Hagenmuller, P. *Z. Anorg. Allg. Chem.* **1993**, *619*, 7.
(43) Demont, A.; Hebert, S.; Pelloquin, D.; Maignan, A. *J. Solid State Chem.* **2008**, *181*, 1314.
(44) Kim, J. H.; Lee, K. T.; Kim, Y. N.; Manthiram, A. *J. Mater. Chem.* **2011**, *21*, 2482.
(45) Shao, Z. P.; Haile, S. M.; Ahn, J.; Ronney, P. D.; Zhan, Z. L.; Barnett, S. A. *Nature* **2005**, *435*, 795.
(46) Zhou, Q. J.; He, T. M.; Ji, Y. J. *Power Sources* **2008**, *185*, 754.
(47) Lee, J. Y.; Swinnea, J. S.; Steinfink, H.; Reiff, W. M.; Pei, S.; Jorgensen, J. D. *J. Solid State Chem.* **1999**, *145*, 116.